ACS OMEGA

http://pubs.acs.org/journal/acsodf

Article

Molecular Dynamics Simulation of the Soret Effect on Two Binary Liquid Solutions with Equimolar *n*-Alkane Mixtures

Jun Zhong,* Renbao Zhao,* Wenze Ouyang, and Shenghua Xu

Cite This: *ACS Omega* 2022, 7, 518−527

Read Online

ACCESS | Metrics & More | Article Recommendations

ABSTRACT: Molecular dynamics is employed to simulate the Soret effect on two binary liquid solutions with equimolar mixtures: normal pentane (*n*-pentane, nC-5) and normal heptane (*n*-heptane, nC-7) molecules plus normal decane (*n*-decane, nC-10) and normal pentane molecules. Moreover, two coarse-grained force field (the CG-FF) potentials, which may depict inter-/intramolecular interactions fairly well among *n*-alkane molecules, are developed to fulfill such investigations. In addition, thermal diffusion for the mass fraction of each of these *n*-alkane molecules is simulated under an effect of a weak thermal gradient (temperature difference) exerting on solution systems from their hot to cold boundary sides. Finally, quantities of the Soret coefficient (SC) for two binary solutions are calculated by means of the developed CG-FF potentials, so as to improve the calculation rationality. As a result, first, it is found that molecules with light molar masses will migrate toward the hot boundary side, while those with heavy molar masses will migrate toward the cold boundary one ; second, the SC quantities indicate that they match relevant experimental determinations fairly well, i.e., trends of these SC quantities show inverse proportionality to the thermal gradient on the systems.

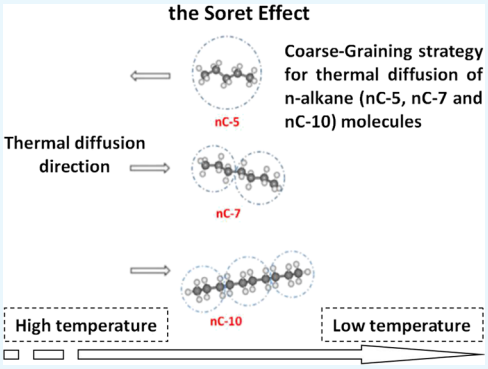

1. INTRODUCTION

Explorations of petroleum resources are of great significance to the development of global economy in human society. In practice, how to effectively delimit a crude oil reservoir underneath still mainly depends upon accurate predictions of distributions for mass fractions of various chemical components in crude oils. According to this, several research institutions in the European Union (EU) have focused on an application of the so-called Soret effect on the oil explorations.[1−15] The Soret effect (the SE), known as one of the important phenomena in thermal diffusion, has been investigated for tens of years. It refers to that, in an isolated and isotropic liquid reservoir, due to the sole effect of a thermal gradient exerting on it (without an effect of gravitation), all the components in the reservoir will evolve their mass fraction distributions accordingly.[1−3] Early lab works have revealed that the Soret coefficient (the SC) quantities used for testing mass fractions of chemical components in the SE should play the main role in exploring crude oil resources.[4−7] However, in practice, it is doubted that distributions for mass fractions of various chemical components in crude oils were influenced by both a thermal gradient and a gravitation.[8−15] Therefore in 2016, "the Sino-EU Cooperative Soret Coefficients in Crude Oil Project" synthesized six sample cells mixing several normal alkane components (*n*-alkane molecules, just having a carbon bough in each molecular conformation) extracted from crude oils. Then, they were sent into space by launching a Chinese SJ-10 retrievable satellite (the SJ-10 Project), so as to make clear if the SC did playthe main role in evolving distributions for mass fractions of *n*-alkane components in crude oils under a very weak gravity field.[16,17]

On the other hand, during the past two decades, with rapid developments of computational algorithms, some modeling methodologies such as molecular dynamics (MD), the Monte Carlo (MC), and the finite element methods (FEM) have shown to be very competent to investigate the SE mechanism in several liquid solutions mixing various chemical components and worked out some amazing outputs. For example, Montel *et al.* investigated the isothermal and nonisothermal properties of some organic liquids by using the MD simulations with the Lennard-Jones (L-J) potentials.[18] They found out that, in the SE, all the components in liquids may have their mass fractions distributed diversely. Touzet *et al.* applied the MD simulations with some simple models (rigid sphere L-J potentials) to a ternary liquid solution mixing methane (nC-1), *n*-butane (nC-4), and *n*-dodecane (nC-12) molecules. They also observed

Received: September 7, 2021
Accepted: December 8, 2021
Published: December 27, 2021

https://doi.org/10.1021/acsomega.1c04926
ACS Omega 2022, 7, 518−527

that, qualitatively, nC-1 and nC-4 molecules would migrate toward the hot region in solution, while nC-12 molecules would migrate toward the cold one.[19] Still, from the SJ-10 Project, Galliéro *et al.* investigated the thermal diffusion for methane (nC-1), *n*-butane (nC-4), and *n*-dodecane (nC-12) molecules in those six sample cells by means of the gas chromatography (GC) and the MD simulations with several simple isotropic plus multipolar L-J potentials. They also found that, qualitatively, nC-1 and nC-4 molecules would gather at the hot-temperature area, but nC-12 molecules would gather at the cold one.[17,20] In addition, Mozaffari *et al.* applied the MD simulations with some simple L-J potentials to the Soret effect on a ternary liquid solution mixing equimolarly *n*-dodecane (nC-12), tetra-hydro-naphthalene, and *iso*-butylbenzene. They calculated the SC quantities and compared them with experimental data from the SJ-10 Project.[21] Unfortunately, they lost some important sample cells from the SJ-10 Project. Thus, their SC quantities could hardly be validated. Overall, all the molecular potentials in the above studies looked quite simple, and relevant simulation objects were too small, so their MD outputs could hardly reveal the essentials of the SC mechanism.

Apparently, one of most important factors to run the MD simulations successfully was how to constitute reliable models of inter-/intramolecular potentials for relevant research objects. For example, during the past two decades, the so-called anisotropic united-atom (AUA) model, which took $-CH_2$, $-CH_3$, and CH_4 as unified interaction sites (hence united atoms) on the conformation of an alkane molecule, has shown excellent competence in many studies.[22−36] To improve the prediction accuracy of inter-/intramolecular potentials among organic molecules, in the MD simulations, Antoun *et al.* investigated the SE on a binary liquid solution mixing nC-5 and nC-10 molecules even by means of a model based upon the all-atom force field.[37] In general, inter-/intramolecular potentials in above studies consisted of five terms: radial stretching, angular bending, torsion (spatial geometry deforming), and van der Waals and electrostatic interactions. Moreover, the AUA model can be viewed as a simplified version of the all-atom force field. However, in practice, for electroneutral *n*-alkane molecules, both torsion and electrostatic terms in the AUA model can be ignored because they played obvious roles only in those alkane isomers (*i*-alkane molecules, having a carbon bough and twigs in each molecular conformation),[36] i.e., for a specific *i*-alkane molecule, the torsion term was found to behave obviously just at the joints where carbon twigs hinged.[39] However, for those macro *n*-alkane (larger than *n*-decane) molecules, adopting the AUA model would increase computational overheads when carrying out the MD simulations. According to this, if we ran the MD simulations for some super large-scale systems (about hundreds of nanometers in size), which were composed of hundreds of thousands of macro alkane molecules in a very long simulation time (hundreds of millions of MD time steps), then we must take a further coarse-graining operation on the conventional AUA model, so as to improve the whole computational efficiency.

In addition, a subsidiary key factor to sustain the MD simulations for the SE on research systems was the so-called nonequilibrium molecular dynamics (the NEMD), which usually adopted an algorithm of the heat-flow exchange between systems and their outside environments (the ΔQ, also the heat convection) in fulfilling simulation processes.[30−35] However, some of the NEMD simulations indicated that the SC quantities showed severe fluctuations at the initial stage when the ΔQ was very small. Then, they would become increasingly stable along with the ΔQ increase, meaning that the ΔQ quantity may have a positive impact on the SC calculations if it increased to quite higher than a certain level.[35] Nevertheless, such a conclusion was quite doubted because thermal fluctuations due to heat convection in experiments usually severely disturbed the accuracy of determining the SC quantity no matter whether the ΔQ quantity was obviously large or not.[38] Therefore, such the NEMD conclusion needed further corroboration.

During the school year 2011, Zhang *et al.* provided some concise coarse-grained beads for depicting real conformations of macro alkane molecules.[39] In their framework, three units of conventional united atoms could even be extended to three larger new ones: $-(CH_2)_2-CH_3$, $-(CH_2)_3-CH_3$, and $-(CH_2)_4-CH_3$. The reason was that, under the standard state, most of the macro alkane molecules were at a liquid state, but conventional united atoms ($-CH_2$, $-CH_3$, and CH_4) were usually at a gaseous state. Thus, the bonding properties of those macro alkane molecules could hardly be represented by conventional ones. However, still under the standard state, $-(CH_2)_2-CH_3$, $-(CH_2)_3-CH_3$, and $-(CH_2)_4-CH_3$ were likely liquefied and were widely regarded as one of the basic debris among macro alkane molecules at a liquid state in petrochemical engineering. According to this, here, new united atoms could be represented by three new coarse-grained beads: A1 ($-(CH_2)_2-CH_3$), A2 ($-(CH_2)_3-CH_3$), and A3 ($CH_3-(CH_2)_3-CH_3$), which may well splice those macro alkane (both *n*-alkane and *i*-alkane) molecules at a liquid state through their effective combinations. Reference 39 indicated that not only may such a coarse-graining strategy depict the colloidal stability of petroleum engineering fairly well but save more computational resources in the MD simulations.

In this article, at first, we constitute two coarse-grained force field (the CG-FF) potentials by means of new united atoms in ref 39. Then, as one of the working extensions in ref 39, the Soret effect on two binary liquid systems with *n*-alkane molecules (nC-5 and nC-7 molecules plus nC-5 and nC-10 molecules) is investigated by using the MD simulations with the developed CG-FF potentials. Our goal is that, if the developed CG-FF potentials here can succeed in carrying out all the MD simulations, then in the future, such techniques for constituting intra-/intermolecular potentials can also be competent to depict other complex molecules (e.g., those super macro alkane isomers) and may bridge very large-scale molecular systems and continuum media.

Figure 1 shows a schematic of real structures of three selected *n*-alkane (nC-5, nC-7, and nC-10) molecules and their geometric modifications spliced by three selected coarse-grained beads (A1, A2, and A3) as mentioned above.

Table 1 lists some physical parameters of the three selected *n*-alkane molecules in nature. In the past, since conventional united atoms can merely provide few pieces of physical and chemical information (e.g., vapor pressures, vaporization enthalpies, and liquid densities) for constituting some relevant inter-/intramolecular potentials in studies,[22−24,26−28] here, we adopt the first-principles calculations (e.g., calculations by using density functional theory, DFT) in optimizing those coarse-grained conformations in Figure 1, which would enrich the fitting information for constituting the CG-FF potentials,

https://doi.org/10.1021/acsomega.1c04926
ACS Omega 2022, 7, 518−527

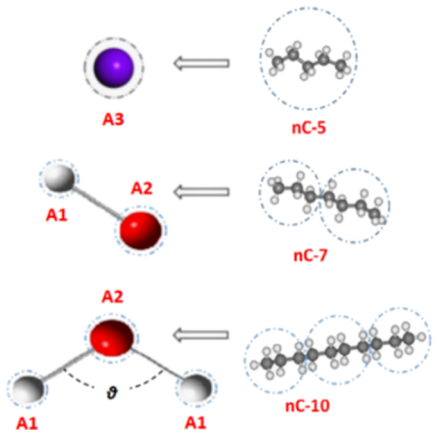

Figure 1. Coarse-grained modifications for real geometrics of three selected *n*-alkane molecules: nC-5, nC-7, and nC-10.

but ref 39 and other works did not adopt them before. That is one novel point in this article.

In our MD framework, to overcome the shortcomings in the NEMD, i.e., to eliminate thermal noise during the NEMD simulations at low temperature levels, we exerted two different temperature quantities (T_1 and T_2, $T_1 > T_2$) on a super cuboid reservoir containing hundreds of thousands of *n*-alkane molecules, from its left through right boundary sides. After running very long MD time steps, both hot- and cold-edge zones could be constructed at two boundary sides so that a quite steady thermal gradient (a temperature difference, $DT = T_1 - T_2$) can be generated to distribute through the edge zones,[41] which may play an equal role to the heat convection in the NEMD. That is another novel point in this article. Please note, here, we do not add an effect of gravitation into all the MD simulations. Moreover, all the MD simulations are under the standard state (e.g., initial pressure = 1.00 atm and initial T_0 = room temperature (299 K)).

This article is organized as follows: Section 2 narrates the MD simulation procedures, Section 3 discusses the MD simulation outputs, Section 4 summarizes the MD simulation results, and Section 5 introduces the methodologies.

2. SIMULATION PROCEDURES

In this article, all the MD simulations were carried out by using the LAMMPS, which is competent to run very large-scale molecular systems.[52] In details, ① initially, each of the MD systems with equimolar mixtures was constructed in a cuboid reservoir, e.g., A3 (nC-5):A1−A2 (nC-7) = 1:1 in a SET-1 system and A3 (nC-5):A1−A2−A1 (nC-10) = 1:1 in a SET-2 system. For the SET-1 system with 36,864 molecules (A3⊕A1−A2), its volume of 600 × 140 × 140 Å^3 was stacked by a dozen of cuboid cells (each cell length in the *x*-direction: 40 Å). Meanwhile, for the SET-2 system with 73,728 molecules (A3⊕A1−A2−A1), its volume of 792 × 176 × 176 Å^3 was stacked by a dozen of cuboid cells (each cell length in the *x*-direction: 44 Å); ② under a periodic boundary condition in the *x*-, *y*-, and *z*-directions, each of the MD systems was equilibrated for approximately 100,000,000 time steps at a desired temperature of 299 K (1 time step = 0.001 ps), plus a hydrostatic pressure (1.00 atm) exerting on the system. This was called the *NPT* ensemble simulation, in which all the relevant coupling parameters are as follows: τ_t = 100 and τ_p = 1000 for the SET-1 system and τ_t = 200 and τ_p = 2000 for the SET-2 system.[41,52] After this step, the resulting volume of the SET-1 system would become 586 × 131 × 131 Å^3, and that of the SET-2 system would become 782 × 174 × 174 Å^3; ③ all the intra-/intermolecular potentials in each of the MD systems were described by the developed CG-FF models in Sections 5.2. The effectiveness of these potentials is shown in Table 2. ④ After thermal equilibrium at a desired temperature (299 K), for each of the MD systems, a hydrostatic pressure (1.00 atm) was still exerting on the system in the *y*- and *z*-directions; meanwhile, in the *x*-direction, there was no pressure to control the system, but two different temperatures (T_1 and T_2, $T_1 > T_2$, $DT = T_1 - T_2$) were applied onto its left and right boundary sides so that hot- and cold-edge zones can be constructed near these two boundary sides to generate a thermal gradient along the *x*-direction.

Table 2. Effectiveness of the CG-FF Models for Two Binary Solutions with Equimolar Mixtures: The SET-1 and the SET-2 Systems

parameters	system	the CG-FF	other works
coefficient of volume thermal expansion (×10^{-3}, K^{-1})	SET-1	0.7063	0.6926[a]
	SET-2	0.4931	0.5065[b]
mass density (g/m^3, 20 °C)	SET-1	0.6760	0.6600[a]
	SET-2	0.7010	0.6900[c]

[a]Data came from ref 40. [b]Data came from ref 53. [c]Data came from ref 58.

Table 1. Some Physical Parameters of *n*-Pentane (nC-5), *n*-Heptane (nC-7), and *n*-Decane (nC-10)[a]

object	*n*-Pentane	*n*-Heptane	*n*-Decane
symbol	nC-5	nC-7	nC-10
molecular formula	CH_3-CH_2-CH_2-CH_2-CH_3	CH_3-CH_2-CH_2-CH_2-CH_2-CH_2-CH_3	CH_3-CH_2-CH_2-CH_2-CH_2-CH_2-CH_2-CH_2-CH_3
molecular geometry	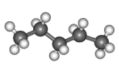	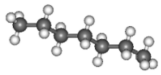	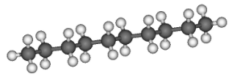
mass density (g/cm^3, 20°C)	0.626	0.680	0.727
molar mass (g/mol)	72.18	100.25	142.35

[a]All relevant data came from refs 39 and 40.

https://doi.org/10.1021/acsomega.1c04926
ACS Omega 2022, 7, 518−527

In details, when simulating an MD system, the *x*-direction was under a free boundary condition, i.e., two vacuum spaces with their own lengths larger than two cutoff distances were set outside its left and right boundary sides, while in the *y*- and *z*-directions, it was still under periodic boundary conditions. As a result, a net thermal pressure due to the *DT* increase may appear in one middle region between two edge zones to drive molecular migrations along the *x*-direction. For example, along the *x*-direction, both hot- and cold-edge zones were controlled by two different external temperatures (e.g., T_1 = 302, 305, and 308 K for the hot-edge zone, but T_2 = 299 K for the cold-edge zone only. Thus, the *DT* between the two edge zones could be set at 3, 6, and 9 K, respectively). However, the middle region in the system would not perform temperature control but allow heat exchange and diffusion along the *x*-direction, which was realized by a constant-energy MD simulation,[41] see Figure 2.

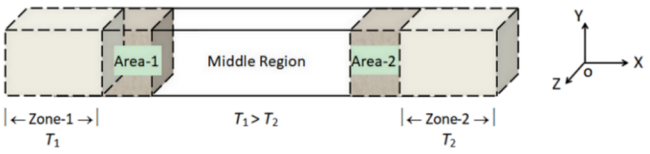

Figure 2. Schematic of the MD simulation geometry.

In Figure 2, both Zone-1 and Zone-2 were named hot- and cold-edge zones, which were controlled by T_1 and T_2, respectively. The middle region between them would perform the heat evolution. In details, for the SET-1 system, along the *x*-direction, each of the two edge zones was set to 93 Å in length, and the middle region was set to 400 Å in length comprising 10 cuboid cells (each cell length along the *x*-direction: 40 Å). Please note, inside the middle region, two areas (Area-1 and Area-2, each of which was set to 120 Å in length) were adjacent to two edge zones, respectively, so that molecular numbers in these two areas could be counted during thermal diffusion. Similarly, for the SET-2 system, along the *x*-direction, each of its two edge zones was set to 172 Å in length, and the middle region was set to 440 Å in length comprising 10 cuboid cells (each cell length along the *x*-direction: 44 Å). Also, inside the middle region, each of the two areas was set to 132 Å in length. Finally, after 500,000,000 time steps of the thermal constraint on the two edge zones, all the MD systems were found to be under the steady state, and the molecular number in each of the 10 cuboid cells in the middle region was counted by an average of 4000 time steps, just for the SC calculations in Section 5.1.

3. RESULTS AND DISCUSSION

3.1. Distribution Trends for Mass Fractions of *n*-Alkane Molecules in Binary Liquid Solutions. Figure 3a shows three distribution (regression) curves representing temperature spatial profiles in the middle region along the *x*-direction in response to three *DT* values between hot- and cold-edge zones in three SET-1 systems (*DT* = 3, 6, and 9 K, and T_2 = 299 K in the cold-edge zone), respectively. Also, Figure 3b shows three distribution (regression) curves representing temperature spatial profiles in the middle region along the *x*-direction in response to three *DT* values between hot- and cold-edge zones in three SET-2 systems (*DT* = 3, 6, and 9 K, and T_2 = 299 K in the cold-edge zone), respectively. In Figure 3, every temperature point was achieved by an average of 4000 time steps after 500,000,000 time steps of the thermal constraint on the two edge zones. Moreover, the solid line was for T_1 = 308 K (*DT* = 9 K), the dashed line was for T_1 = 305 K (*DT* = 6 K), and the dash-dotted line was for T_1 = 302 K (*DT* = 3 K). From Figure 3, it may be concluded that, under the steady state, the increase in the thermal gradient was well exerting on those SET systems to promote molecular migrations during the whole thermal diffusion.

Figure 4 shows three distributions for nC-5 mass fractions (M_f, also the relevant C_i) in the middle region along the *x*-direction corresponding to three *DT* values (*DT* = 3, 6, and 9 K) between hot- and cold-edge zones in three SET-1 systems, respectively. In this figure, every point was achieved from calculations in the Appendix. Three slopes representing distribution trends for the M_f were determined by the linear regression. From this figure, it can be seen that the larger the temperature difference (*DT*) on the system (being an effect of the thermal gradient), the steeper the M_f slope and the smaller the M_f fluctuations became, and thus, the bigger the driving effect on nC-5 molecular migrations during thermal diffusion. Overall, three M_f slopes corresponding to three *DT* values were shown to be declining gradually, meaning that more nC-5 molecules (with light molar mass) would migrate into the hot area (Area-1) than the cold one (Area-2) with the *DT* increase.

Figure 5 shows three distributions for nC-5 mass fractions (M_f, also the relevant C_i) in the middle region along the *x*-direction corresponding to three *DT* values (*DT* = 3, 6, and 9 K) between hot- and cold-edge zones in three SET-2 systems, respectively. In this figure, every point was achieved from calculations in the Appendix. Three slopes representing distribution trends for the M_f were determined by the linear regression. From this figure, it can also be seen that the larger the temperature difference (*DT*) on the system (being an effect of the thermal gradient), the steeper the M_f slope and the

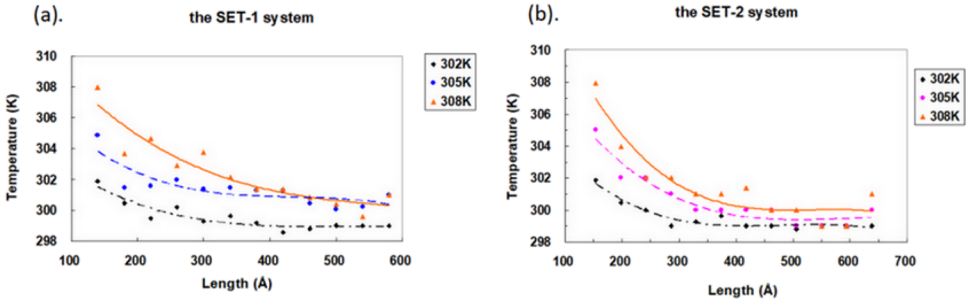

Figure 3. Distribution (regression) curves representing temperature spatial profiles in the middle region along the *x*-direction corresponding to three temperature differences (*DT* of 3, 6, and 9 K): (a) three SET-1 systems and (b) three SET-2 systems.

https://doi.org/10.1021/acsomega.1c04926
ACS Omega 2022, 7, 518−527

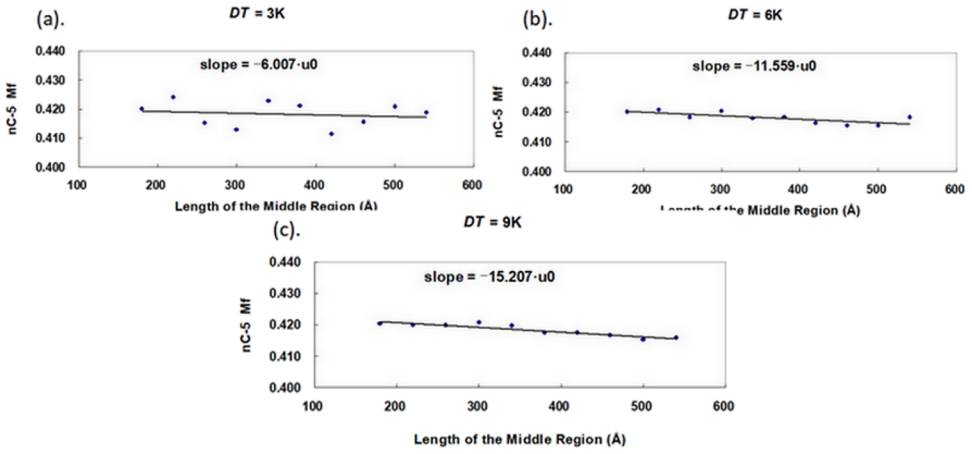

Figure 4. Distributions for nC-5 mass fractions (M_f) in the middle region in three SET-1 systems ($u_0 = 10^{-6}$): (a) DT = 3 K, (b) DT = 6 K, and (c) DT = 9 K.

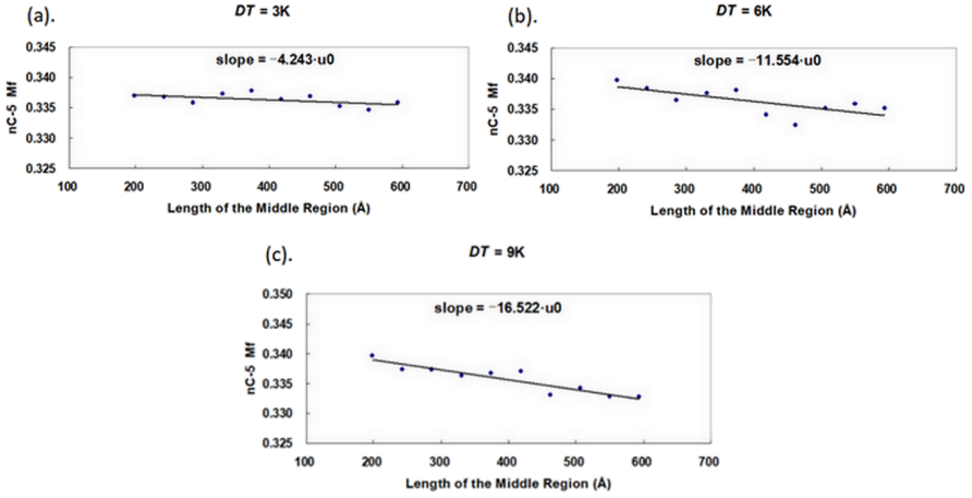

Figure 5. Distributions for nC-5 mass fractions (M_f) in the middle region in three SET-2 systems ($u_0 = 10^{-6}$): (a) DT = 3 K, (b) DT = 6 K, and (c) DT = 9 K.

smaller the M_f fluctuations became, and thus, the bigger the driving effect on nC-5 molecular migrations during thermal diffusion. Overall, three M_f slopes corresponding to three DT values were shown to be declining gradually, meaning that more nC-5 molecules (with light molar mass) would migrate into the hot area (Area-1) than the cold one (Area-2) with the DT increase.

Apparently, Figures 4 and 5 may corroborate what the NEMD did before,[31−35] i.e., a thermal gradient (equivalent to the heat-flow exchange) had a positive impact on the Soret effect if it increased to higher than a certain level. Thus, increasing the thermal gradient could be fairly effective to the SC calculations because a linear response and constant phases in the MD simulations can be well ensured under this higher constraint, while they could hardly be well determined in relevant experimental works.

Mechanisms of thermal diffusion in Figures 4 and 5 could be explained as follows: In each of the two binary liquid solutions here, from data in Table 5, it may receive the following: ε [nC-5⊕nC-7] = −0.06328 eV > $\frac{1}{2}[\varepsilon$ (nC-5) + ε (nC-7)] = −0.06740 eV and ε [nC-5⊕nC-10] = −0.06319 eV > $\frac{1}{2}[\varepsilon$ (nC-5) + ε (nC-10)] = −0.06733 eV, meaning that there were very weak hydrophobic associations between nC-5 and nC-7 molecules and between nC-5 and nC-10 molecules, even if these two binary liquid solutions looked uniform. In addition, geometric differences between nC-5 and nC-7 molecules and between nC-5 and nC-10 molecules were both more than 15%. Therefore, when the thermal gradient was increasingly applied onto each of the SET systems, all the molecules in the systems would perform their thermal migrations by means of severe molecular collisions.[25] For example, in Area-1 (near the hot-edge zone), it was quite easier for more nC-5 molecules (with light molar mass) than nC-7 and nC-10 molecules (both with heavy molar masses) to have their own thermal segregation. As a result, some of nC-7 or nC-10 molecules in Area-1 were squeezed out of this area but migrated toward inner sites of the middle region. Consequently, vacancies in Area-1 due to heavy molecular leaving would likely attract more nC-5 molecules from the middle region to fill in. Then, *new vacancies* would appear in the middle region due to nC-5 molecular leaving. Simultaneously, those heavy nC-7 and nC-10 molecules squeezed out of Area-1 but flowing into the middle region could partially fill in those *new vacancies* because of their obvious geometric differences with nC-5 molecules. Accordingly, the remaining *new vacancies* in the middle region would attract some other nC-5 molecules as well from Area-2 (near the cold-edge zone) to fill in. Following this migration path,

https://doi.org/10.1021/acsomega.1c04926
ACS Omega 2022, 7, 518−527

Table 3. Three SC Quantities for SET-1 and SET-2 Systems Corresponding to Three Temperature Differences[a]

temperature difference between hot- and cold-edge zones, DT (K)		3 (T_1 = 302 K)	6 (T_1 = 305 K)	9 (T_1 = 308 K)
the Soret coefficient ($\times 10^{-3}$, K^{-1})	SET-1	−3.17 ± 0.14	−2.36 ± 0.17	−2.08 ± 0.20
	SET-2	−3.45 ± 0.19	−2.61 ± 0.20	−2.33 ± 0.13

[a] T_2 = 299 K in cold Zone-2, while T_1 in hot Zone-1 are listed in the table.

some nC-7 or nC-10 molecules in the middle region were also squeezed out of this region but migrated toward Area-2. At the final steady state (after 500,000,000 time steps of the thermal constraint on the two edge zones), nC-5 molecules would be abundant in Area-1 (near hot Zone-1), while nC-7 and nC-10 molecules would be affluent in Area-2 (near cold Zone-2). Obviously, more nC-7 and more nC-10 molecules (both with heavy molar masses) in the SET systems were found to have their thermal migrations opposite to the nC-5 molecules with the DT increase, which were also observed in other works.[17−19]

3.2. Calculations of the Soret Coefficients. By using eq 4, three SC quantities for nC-5 molecules in three SET-1 systems corresponding to three DT values in Figure 4 were calculated. In addition, three SC quantities for nC-5 molecules in three SET-2 systems corresponding to three DT values in Figure 5 were calculated. Please note, here, T_2 = 299 K was taken as a reference point, and the M_f quantities in Area-1 and Area-2 were selected for the SC calculations by means of the optimized interpolation.[35,39] Table 3 lists relevant results for these SC quantities. From this table, it may be concluded that the SC quantities for nC-5 molecules in both the SET-1 and the SET-2 systems would decline gradually along with the DT increase.

Still coming back to eq 3, along the x-direction, since the C_i was the T-dependent, an indefinite integral solution for this equation: $S_T^i = -\frac{1}{T}\left[\text{constant} + \ln\left(\frac{C_i}{1-C_i}\right)\right]$ may represent a function of the $\frac{1}{T}$ variable. To approve of this point, Figure 6 shows two trends of the SC quantities for nC-5 molecules versus the temperature difference ($DT = T - T_0$) on the SET-1 and the SET-2 systems. Relevant data in this figure came from Table 3, and T_0 = 299 K was taken as the reference point. From Figure 6, it may be observed that two trends of the SC quantities for nC-5 molecules in the two SET systems were both inversely proportional to the DT value (corresponding to the thermal gradient). Also, from this figure, the SC on the SET-2 system was found to perform more obviously than on the SET-1 system.

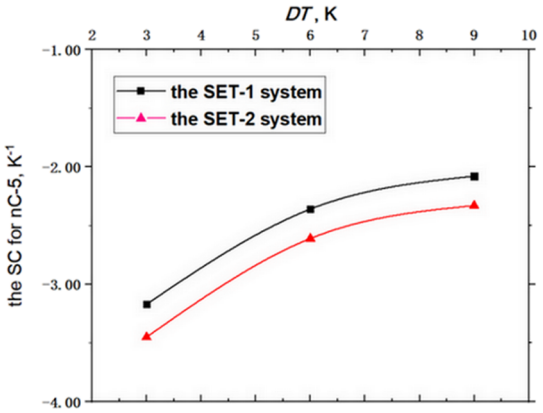

Figure 6. Two trends of the SC quantities for nC-5 molecules corresponding to three temperature differences in the SET-1 and SET-2 systems.

In experimental works, the SC quantity for a binary liquid solution was usually represented by its absolute value. Thus, qualitatively, Dominguez *et al.* reported that an expression of the Soret coefficient (absolute value) for an isotopic fractional element (the melting silicate) under a thermal gradient showed a function of the inverse of the absolute temperature if choosing the zero point as the temperature reference point.[54] Essentials of such curve distributions in Figure 6 could be explained as follows: According to the SC definition, $S_T = \frac{D_T}{D_C}$, in a uniform liquid solution, the D_T usually became blunt if the thermal gradient did not severely impact the system (e.g., just ±1 K deviation at each temperature point in Figure 3 may represent a very low phonon excitation). However, the D_C was fairly sensitive to the thermal gradient even if the latter just behaved a small alteration (see obvious M_f fluctuations in Figures 4 and 5). On the whole, the S_T quantity would be declining if the thermal gradient was increasing gradually. In addition, three other works also reported that:[55−57] if a multicomponent system was under an effect of a thermal gradient, then lighter fractional elements would concentrate in the hot region, while heavier elements would concentrate in the cold one. According to them, qualitatively, trends of the SC quantity versus the temperature difference, and trends of molecular migrations under influences of the thermal gradient on the SET systems here, would be in good agreement with those of the experimental observations.

Still, in experimental works, quantitatively, Leahy-Dios and Firoozabadi reported that an SC quantity (absolute value) for a binary liquid solution with equal-weight (50 wt %) nC5−nC10 mixtures would lay in [3.66, 4.06] × 10^{-3} K^{-1}, mainly dependent upon different molecular shapes and sizes (normal and isomer molecular conformations) in the system.[53] In Perronace *et al.*'s work,[27] starting from 300 K, one SC quantity (absolute value) for a multicomponent C5−C10 system with equimolar mixtures would lay in [2.76, 4.42] × 10^{-3} K^{-1}. In addition, starting from 298 K, Mounir Bou-Ali *et al.* determined the SC quantities for several binary liquid solutions mixing various n-alkane molecules.[58] In their works, the SC quantity for a binary solution with equimolar nC-5 and nC-10 mixtures was 2.96 × 10^{-3} K^{-1} if an obvious thermal flow passed through the whole system. Compared with the above results, for the SET-2 system, its SC quantities obtained from the MD simulations here, (2.33−3.45) × 10^{-3} K^{-1}, would match those works fairly well.

Unfortunately, there were no relevant reports about the SC quantity for the SET-1 system. However, in ref 58, the SC quantities of four equimolar mixtures, nC-7 and nC-10, nC-10 and nC-14, nC-12 and nC-17, and nC-13 and nC-18, were determined. Their values were 1.87 × 10^{-3}, 2.17 × 10^{-3}, 2.40 × 10^{-3}, and 2.35 × 10^{-3} K^{-1}, respectively. Since the ratio of carbon atoms between two components in each of the four mixtures above was within [1.38, 1.42], all of which were near that in the SET-1 system (nC-5⊕nC-7), the SC quantities for

https://doi.org/10.1021/acsomega.1c04926
ACS Omega 2022, 7, 518−527

the SET-1 system obtained from the MD works here, (2.08 ~ 3.17) × 10^{-3} K^{-1}, would also match those findings.

4. CONCLUSIONS

At the nanoscale, coarse-grained molecular dynamics (MD) was fulfilled to simulate the Soret effect (SE) on two binary liquid solutions with equimolar mixtures: *n*-pentane (nC-5) and *n*-heptane (nC-7) molecules plus *n*-pentane (nC-5) and *n*-decane (nC-10) molecules. Some results can be drawn as follows:

First, before the MD simulations, two coarse-grained force field (the CG-FF) potentials, which were based upon a model of new united atoms, were developed to depict intra-/intermolecular interactions in the above liquid solutions. As a result, they were quite reliable throughout the whole MD simulations.

Second, under an effect of a weak thermal gradient on the two systems, the MD simulations indicated that nC-5 molecules with light molar mass would migrate toward the high-temperature region, while nC-7 and nC-10 molecules with heavy molar masses would migrate toward the low-temperature region, both of which were also observed in other relevant works. In addition, the higher the thermal gradient on two systems, the more obvious the SE would be. Mechanisms of such phenomena were mainly due to very weak hydrophobic associations between two different types of *n*-alkane molecules in each of the binary liquid solutions.

Third, still under the effect of a weak thermal gradient, quantities of the Soret coefficient (SC) for the above binary liquid solutions were calculated by means of the developed CG-FF potentials. Calculations were found to match other relevant works fairly well. In addition, trends of the SC quantity versus the temperature difference on the systems looked inversely proportional.

Finally, the fact that the SE outputs corroborated fairly well with other relevant works here may support that our developed CG-FF potentials have opened a good perspective: in the future, they may play a very promising role in simulating other relevant properties of petroleum engineering.

5. METHODOLOGIES

5.1. Equations of Thermal Diffusion. In a cuboid reservoir containing a uniform liquid solution mixing various components, under an effect of a thermal gradient (temperature difference) from hot to cold boundary sides of the reservoir, mass fractions of these components would distribute accordingly.[2−4] Assuming that a uniform liquid system just consists of two components, thus, a comprehensive flux for component *i* should obey the following diffusion law[2]

$$J_i = -\rho_i D_C^i \nabla C_i - \rho_i D_T^i C_i(1 - C_i)\nabla T \tag{1}$$

where T is a thermal temperature field exerting on the system, C_i is a mass fraction for component i in response to the T variable, ρ_i is a mass density for component i, and D_T^i and D_C^i represent two rates of thermal diffusion and mass diffusion for component i, respectively. When the system reaches the steady state (i.e., the $J_i = 0$), the T and the C_i would distribute steadily. In this case, eq 1 could be converted as follows

$$\nabla C_i = -\frac{D_T^i}{D_C^i} C_i(1 - C_i)\nabla T = -S_T^i C_i(1 - C_i)\nabla T \tag{2}$$

where $S_T^i = \frac{D_T^i}{D_C^i}$, denoting a definition of the Soret coefficient (SC) for component i, and its unit is K^{-1}. In practice, if considering the SE along the x-direction only, then eq 2 will have its projection on the x-axis as an ordinary differential equation, i.e.,

$$\frac{dC_i}{dx} = -S_T^i C_i(1 - C_i)\left(\frac{dT}{dx}\right) \tag{3}$$

Generally, eq 3 may well depict the characteristic of thermal diffusion in most of the macro systems with uniform liquids. However, if the size of a system is around the nanoscale and the thermal gradient exerting on the system is quite weak, then both the D_T^i and the D_C^i would perform gently.[42] In this case, the S_T^i could be viewed as a constant throughout the whole system. Therefore, along the x-direction, if setting up hot (T_1)- and cold (T_2)-edge zones at the left and right boundary sides of the system ($T_1 > T_2$) and naming C_i^h the mass fraction for component i in an area adjacent to the hot-edge zone and C_i^l the one adjacent to the cold-edge zone, by solving eq 3 with the method of variable separation, then the S_T^i for component i can be derived as follows

$$S_T^i = \frac{1}{(T_1 - T_2)} \ln\left[\frac{C_i^l(1 - C_i^h)}{C_i^h(1 - C_i^l)}\right] \tag{4}$$

Please note, at the final steady state, both the C_i^h and the C_i^l must have accumulated all information of the C_i evolution throughout the whole thermal diffusion.

5.2. Models Selected for the MD Simulations. In the MD simulations here, two uniform binary liquid solutions with equimolar mixtures: the SET-1 system with nC-5 and nC-7 molecules and the SET-2 system with nC-5 and nC-10 molecules, were selected for the studied objects.

As discussed in Section 1, both the AUA and the all-atom force field models usually consisted of two main terms

$$E_{tot} = E_{bond} + E_{nonbond} \tag{5}$$

where E_{bond} represented strong intramolecular chemical bonds (atomic bonds in one molecular conformation) and $E_{nonbond}$ represented weak intermolecular interactions among all the molecular groups. In details, (a) the E_{bond} term consisted of three subterms

$$E_{bond} = E_{radial} + E_{angle} + E_{torsion} \tag{6}$$

where $E_{radial} = k_r(r - r_0)^2$, a harmonic model denoting an effect of radial stretching (k_r was a radial strength, and r_0 was an initial radial quantity), $E_{angle} = k_\theta(\theta - \theta_0)^2$, a harmonic model denoting an effect of angular bending (k_θ was an angular strength, and θ_0 was an initial angular quantity), and $E_{torsion} = E_{dihedral} + E_{off\text{-}plane}$, denoting a deforming effect of spatial geometry. Here, k_r, r_0, k_θ, and θ_0 are empirical parameters.

(b) The $E_{nonbond}$ term consisted of two subterms

$$E_{nonbond} = E_{vdW} + E_{electric} \tag{7}$$

where the E_{vdW} denoted van der Waals interactions and the $E_{electric}$ denoted electrostatic interactions.

(c) For each of the electroneutral *n*-alkane molecules, both the $E_{torsion}$ and the $E_{electric}$ contributions would become secular. Thus, eq 5 can be simplified as follows

$$E_{tot} = E_{radial} + E_{angle} + E_{vdW} \tag{8}$$

https://doi.org/10.1021/acsomega.1c04926
ACS Omega 2022, 7, 518−527

Table 4. The Fitting Parameters for the Bonding Status in the Coarse-Grained Beads

		bond strength		bond geometry		
bead type	potential model	radial k_r [eV/Å^2]	angular k_θ [eV/(°)^2]	length r_0 [eV/Å^2]	angular θ_0 [°]	bead molar mass [g/mol]
A1−A2	the CG-FF	28.998		4.193		44.107−58.138
A1−A2−A1	the CG-FF	28.998	0.4129	4.193	179.6	44.107−58.138−44.107
another calculation[a]		25.911	0.5183	4.180	180.0	

[a]Data came from ref 39.

Equation 8 may represent the CG-FF model in this article. Overall, from this model, one nC-7 molecule was spliced by an A1−A2 group, one nC-10 molecule was spliced by an A1−A2−A1 group, and one nC-5 molecule was depicted by an A3 bead only.[39,42] By means of the DFT calculations,[43−45] the empirical parameters k_r, r_0, k_θ, and θ_0 in the E_{radial} and the E_{angle} terms were determined by using the Birch−Murnaghan equation of state (BMES) at its harmonic stage.[46,47] Table 4 lists all the fitting parameters for these two terms in A1−A2 and A1−A2−A1 groups as shown in Figure 1.

Still, in eq 8, the E_{vdW} term was represented by an L-J potential, $E_{vdW} = 4\varepsilon\left[\left(\frac{\sigma}{r}\right)^{12} - \left(\frac{\sigma}{r}\right)^{6}\right]$, where ε and σ were empirical parameters. Table 5 lists all the fitting parameters

Table 5. The Fitting Parameters to Represent van der Waals Interactions among A1, A2, and A3 Beads[b]

bead type	potential model	bond strength ε (eV)	bond strength σ (Å)	bead molar mass (g/mol)
A1−A1[a]	L-J	−0.04381	5.1276	44.107−44.107
A1−A2	L-J	−0.14420	5.5289	44.107−58.138
A1−A3	L-J	−0.06300	5.5835	44.107−72.169
A2−A2[a]	L-J	−0.04459	5.9302	58.138−58.138
A2−A3	L-J	−0.06356	5.9848	58.138−72.169
A3−A3[a]	L-J	−0.09059	6.0395	72.169−72.169

[a]Data came from ref 39. [b]Please note, there is no L-J interaction between A1 and A2 beads inside each single molecule.

in those E_{vdW} terms for A1, A2, and A3 bead interactions (intermolecular potentials) as shown in Figure 1. The cutoff distance of the potential tail in each of the E_{vdW} terms was chosen as 12.00 Å. In Table 5, values of ε and σ for A1−A1, A2−A2, and A3−A3 beads were chosen from refs 39 and 47−49. However, ε values for A1−A2, A1−A3, and A2−A3 beads were obtained from those for A1−A1, A2−A2, and A3−A3 beads by using the geometric mean method. Also, σ values for A1−A2, A1−A3, and A2−A3 beads were obtained from those for A1−A1, A2−A2, and A3−A3 beads by using the arithmetic mean method. Regarding validations of these mean methods, see refs 50 and 51 .

A. APPENDIX

In this article, by means of some skills in Materials Studio 7.0[59] and GROMACS,[60] two uniform binary liquid solutions with equimolar *n*-alkane mixtures were constructed through generating molecules one by one in each of two cuboid reservoirs with super large sizes. Then, as discussed in Section 2, after the *NPT* ensemble simulations by using the LAMMPS, the C_i values for those subcuboid cells in each of the super cuboid systems may be obtained in the following steps:

For example, in a uniform binary liquid solution with equimolar mixtures, *n*-pentane (nC-5) and *n*-heptane (nC-7) molecules, the number of nC-5 molecules in one of the subcuboid cells is named N_5, and that of nC-7 molecules is named N_7, with molar masses M_5 = 72.18 g/mol and M_7 = 100.25 g/mol and the Avogadro constant N_{avo}. Thus, the nC-5 mass fraction (the C_5) in the subcuboid cell can be calculated as follows[42]

$$C_5 = \frac{\frac{N_5}{N_{avo}} \times M_5}{\frac{N_5}{N_{avo}} \times M_5 + \frac{N_7}{N_{avo}} \times M_7} = \frac{N_5 \times M_5}{N_5 \times M_5 + N_7 \times M_7} \quad (9)$$

Similarly, the C_7 quantity in the subcuboid cell can be derived from eq 9 by replacing $N_5 \cdot M_5$ with $N_7 \cdot M_7$ in the numerator. Also, the C_{10} quantity in an nC-5 and nC-10 system may follow the same way as above.

AUTHOR INFORMATION

Corresponding Authors

Jun Zhong − *College of Materials Engineering, North China Institute of Aerospace Engineering, Langfang 065000, P.R. China*; orcid.org/0000-0002-5168-1729; Email: settings83@hotmail.com

Renbao Zhao − *College of Petroleum Engineering, China University of Petroleum Beijing, Beijing 102249, P.R. China*; Email: zhaorb@cup.edu.cn

Authors

Wenze Ouyang − *Institute of Mechanics, Chinese Academy of Sciences, Beijing 100190, P.R. China*

Shenghua Xu − *Institute of Mechanics, Chinese Academy of Sciences, Beijing 100190, P.R. China*; orcid.org/0000-0001-5433-0409

Complete contact information is available at: https://pubs.acs.org/10.1021/acsomega.1c04926

Author Contributions

The research work was done through the contributions of all authors. All authors have given approval to the final version of the manuscript.

Notes

The authors declare no competing financial interest.

ACKNOWLEDGMENTS

This work was sponsored by the National Science Foundation (grant no. DMR9619353), USA, the National Natural Science Foundation of China (grant nos. U1738108, 11972348, and 22172180), the Youth Fund for Colleges and Universities in Hebei Province Science and Technology Research Project (grant no. QN2019221), and the Hebei Provincial Key Laboratory of Thermal Protection Materials (SZX2020038, in preparation), China. The authors also acknowledge Mr. Jinming Wang and Ms. Yifang Cui for their valuable efforts on this work.

https://doi.org/10.1021/acsomega.1c04926
ACS Omega 2022, 7, 518−527

REFERENCES

(1) Farber, M.; Libby, W. F. Effect of Gravitational Field on the Thermal Diffusion Separation Method. *J. Chem. Phys.* **1940**, *8*, 965−969.

(2) de Groot, S.R.; Mazur, P. *Nonequilibrium Thermodynamics*; Dover Publication Inc: New York, 1953.

(3) Danby, C. J.; Lambert, J. D.; Mitchell, C. M. Separation of Hydrocarbon Isomers by Thermal Diffusion. *Nature* **1956**, *177*, 1225−1226.

(4) Butler, B. D.; Turner, J. C. R. Flow-cell studies of thermal diffusion in liquids. Part 1 - Cell construction and calibration. *Trans. Faraday Soc.* **1966**, *62*, 3114−3120.

(5) Horne, F. H.; Bearman, R. J. Thermogravitational Thermal Diffusion in Liquids. I. The Formal Theory. *J. Chem. Phys.* **1962**, *37*, 2842−2857.

(6) Horne, F. H.; Bearman, R. J. Thermogravitational Thermal Diffusion in Liquids. II. Experimental Thermal Diffusion Factors for Carbon Tetrachloride Cyclohexane at 25°C. *J. Chem. Phys.* **1962**, *37*, 2857−2872.

(7) Giglio, M.; Vendramini, A. Thermal-Diffusion Measurements near a Consolute Critical Point. *Phys. Rev. Lett.* **1975**, *34*, 561−564.

(8) Kolodner, P.; Williams, H.; Moe, C. Optical measurement of the Soret coefficient of ethanol/water solutions. *J. Chem. Phys.* **1988**, *88*, 6512−6524.

(9) Montel, F. Importance de la thermodiffusion en exploration et production pétrolières. *Entropie* **1994**, *30*, 84−93.

(10) Zhang, K. J.; Briggs, M. E.; Gammon, R. W.; Sengers, J. V. Optical measurement of the Soret Coefficient and the diffusion coefficient of liquid mixtures. *J. Chem. Phys.* **1996**, *104*, 6881−6892.

(11) Høier, L.; Whitson, C. H. Compositional grading - theory and practice. *SPE Reservoir Eval. and Eng.* **2001**, *4*, 525−535.

(12) Ghorayeb, K.; Firoozabadi, A.; Anraku, T. Interpretation of the unusual fluid distribution in the Yufutsu gas-condensate field. *SPE Journal* **2003**, *8*, 114−123.

(13) Platten, J. K. The Soret Effect: A Review of Recent Experimental Results. *J. Appl. Mech.* **2006**, *73*, 5−15.

(14) Montel, F.; Bickert, J.; Lagisquet, A.; Galliéro, G. Initial state of petroleum reservoirs: A comprehensive approach. *J. Pet. Sci. Eng.* **2007**, *58*, 391−402.

(15) Rahman, M. A.; Saghir, M. Z. Thermodiffusion or Soret Effect: Historical review. *Int. J. Heat Mass Tranfer* **2014**, *73*, 693−705.

(16) Xu, S. H. The SCCO Project in the SJ-10 Retrievable Satellite. *Mech. in Eng.* **2016**, *38*, 215−216.

(17) Galliéro, G.; Bataller, H.; Xu, S. H. Thermodiffusion in multicomponent n-alkane mixtures. *Npj Microgravity* **2017**, *3*, 20−27.

(18) Montel, F.; Galliéro, G.; Montel, F. Non-Isothermal gravitational segregation by molecular dynamics simulations. *Phys. Rev. E.* **2008**, *78*, No. 041203.

(19) Touzet, M.; Galliéro, G.; Lazzeri, V. Thermodiffusion: From microgravity experiments to the initial state of petroleum reservoirs. *C. R. Mec.* **2011**, *339*, 318−323.

(20) Galliéro, G.; Bataller, H.; Croccolo, F.; Vermorel, R.; Artola, P.-A.; Rousseau, B.; Vesovic, V.; Bou-Ali, M.; de Zárate, J. M. O.; Xu, S.; Zhang, K.; Montel, F. Impact of Thermodiffusion on the Initial Vertical Distribution of Species in Hydrocarbon Reservoirs. *Microgravity Sci. Technol.* **2016**, *28*, 79−86.

(21) Mozaffari, S. H.; Srinivasan, S.; Saghir, M. Z. A study on thermodiffusion in ternary liquid mixtures using enhanced molecular dynamics algorithm with experimental validation. *Canad. J. Chem. Eng.* **2018**, *97*, 2344−2350.

(22) Toxvaerd, S. R. Molecular dynamics calculation of the equation of state of alkanes. *J. Chem. Phys.* **1990**, *93*, 4290−4295.

(23) Padilla, P.; Toxvaerd, S. Self-diffusion in n-alkane fluid models. *J. Chem. Phys.* **1991**, *94*, 5650−5654.

(24) Toxvaerd, S. Equation of state of alkanes II. *J. Chem. Phys.* **1997**, *107*, 5197−5204.

(25) Dysthe, D. K.; Fuchs, A. H.; Rousseau, B. Fluid transport properties by equilibrium molecular dynamics. I. Methodology at extreme fluid states. *J. Chem. Phys.* **1999**, *110*, 4047−4059. *ibid.* **1999**, *110*, 4060-4067; *ibid.* **2000**, *112*, 7581-7590

(26) Ungerer, P.; Beauvais, C.; Delhommelle, J.; Boutin, A.; Rousseau, B.; Fuchs, A. H. Optimization of the anisotropic united atoms intermolecular potential for n-alkanes. *J. Chem. Phys.* **2000**, *112*, 5499−5510.

(27) Perronace, A.; Leppla, C.; Leroy, F.; Rousseau, B.; Wiegand, S. Soret and mass diffusion measurements and molecular dynamics simulations of n-pentane and n-decane mixtures. *J. Chem. Phys.* **2002**, *135*, 3178−3729.

(28) Boutard, Y.; Ungerer, P.; Teuler, J. M.; Ahunbay, M. G.; Sabater, S. F.; Mackie, A. D.; Pérez-Pellitero, J.; Bourasseau, E. Extension of the anisotropic united atoms intermolecular potential to amines, amides and alkanols: Application to the problems of the 2004 Fluid Simulation Challenge. *Fluid Phase Equilib.* **2005**, *236*, 25−41.

(29) Nieto-Draghi, C.; Bocahut, A.; Creton, B.; Have, P.; Ghoufi, A.; Wender, A.; Boutin, A.; Rousseau, B.; Normanda, L. Optimisation of the dynamical behaviour of the anisotropic united atom model of branched alkanes: application to the molecular simulation of fuel gasoline. *Mol. Simul.* **2008**, *34*, 211−230.

(30) Allen, W.; Rowley, R. L. Predicting the viscosity of alkanes using nonequilibrium molecular dynamics: Evaluation of intermolecular potential models. *J. Chem. Phys.* **1997**, *106*, 10273−10281.

(31) Nieto-Draghi, C.; Ávalos, J. B.; Rousseau, B. Computing the Soret coefficient in aqueous mixtures using boundary driven nonequilibrium molecular dynamics. *J. Chem. Phys.* **2005**, *122*, 114503.

(32) Perronace, A.; Simon, J. M.; Rousseau, B.; Ciccotti, G. Flux expressions and NEMD perturbations for models of semi-flexible molecules. *Mol. Phys.* **2001**, *99*, 1139−1149.

(33) Zhang, M.; Müller-Plathe, F. Reverse nonequilibrium molecular-dynamics calculation of the Soret coefficient in liquid benzene/cyclohexane mixtures. *J. Chem. Phys.* **2005**, *123*, 124502.

(34) Köhler, W.; Morozov, K. I. The Soret Effect in Liquid Mixtures - A Review. *J. Non-Equilib. Thermodyn.* **2016**, *41*, 151−197.

(35) Chen, X.; Liang, R.; Wang, Y.; Xia, Z.; Cui, G. A theoretical study of the temperature gradient effect on the Soret coefficient in n-pentane/n-decane mixtures using non-equilibrium molecular dynamics. *J. Non-Equilib. Thermodyn.* **2020**, *45*, 319−332.

(36) Olivet, A.; Vega, L. F. Optimized molecular force field for sulfur hexafluoride simulations. *J. Chem. Phys.* **2007**, *126*, 144502.

(37) Antoun, S.; Saghir, M. Z.; Srinivasan, S. An improved molecular dynamics algorithm to study thermodiffusion in binary hydrocarbon mixtures. *J. Chem. Phys.* **2018**, *148*, 104507.

(38) Firoozabadi, A. *Thermodynamics and Applications in Hydrocarbon Energy Production*; McGraw-Hill Education: New York, 2016.

(39) Zhang, H. Y.; Wang, Y. Y.; Gui, B. Coarse-grained molecular mechanics (MM) / molecular dynamics (MD) force field for petroleum chemistry: I. Coarse-grained model for alkanes in petroleum. *Acta Chim. Sin.* **2011**, *69*, 2053−2062.

(40) Anslyn, E.V.; Dougherty, D.A. *Modern Physical Organic Chemistry*; University Science Books: New York, 2006.

(41) Hoover, W. *Computational Statistical Mechanics*; Elsevier: Amsterdam, 1991.

(42) Cengel, Y.A.; Ghajar, A.J. *Heat and Mass Transfer: Fundamentals and Applications*, 5th ed., Mc Graw Hill: New York, 2011.

(43) Bear, J. E.; Svitkina, T. M.; Krause, M.; Schafer, D. A.; Loureiro, J. J.; Strasser, G. A.; Maly, I. V.; Chaga, O. Y.; Cooper, J. A.; Borisy, G. G.; Gertler, F. B. Antagonism between Ena/VASP proteins and actin filament capping regulates fibroblast motility. *Cell* **2002**, *109*, 509−521.

(44) Zhong, J.; Hector, L. G., Jr.; Adams, J. B. Dynamic decomposition of aliphatic molecules on Al(111) from ab initio molecular dynamics. *Phys. Rev. B* **2009**, *79*, 125419.

(45) Zhong, J.; Adams, J. B. Adsorption and decomposition pathways of Vinyl-Phosphonic and Ethanoic-Acids on the Al (111) surface: a density functional analysis. *J. Phys. Chem. C* **2007**, *111*, 7366−7375.

https://doi.org/10.1021/acsomega.1c04926
ACS Omega 2022, 7, 518−527

(46) Murnaghan, F. D. The Compressibility of Media under Extreme Pressures. *Proc. Natl. Acad. Sci. U. S. A.* **1944**, *30*, 244−247.
(47) Birch, F. Finite Elastic Strain of Cubic Crystals. *Phys. Rev.* **1947**, *71*, 809−824.
(48) Marrink, S. J.; de Vries, A. H.; Mark, A. E. Coarse-grained model for semiquantitative lipid simulations. *J. Phys. Chem. B* **2004**, *108*, 750−760.
(49) Baron, R.; Trzesniak, D.; de Vries, A. H.; Marrink, S. J. Comparison of thermodynamic properties of coarse-grained and atomic-level simulation models. *ChemPhysChem* **2007**, *8*, 452−461.
(50) Prausnitz, J. M.; Lichtenthaler, R. N.; de Azevedo, E. G. *Molecular thermodynamics of fluid-phase equilibria*; 3rd ed., Prentice Hall: New Jersey, 1999.
(51) Voth, G. A. *Coarse-graining of condensed phase and biomolecular systems*; CRC press: New York, 2008, DOI: 10.1201/9781420059564.
(52) https://lammps.sandia.gov/.
(53) Leahy-Dios, A.; Firoozabadi, A. Molecular and thermal diffusion coefficients of alkane-alkane and alkane-aromatic binary mixtures: Effect of shape and size of molecules. *J. Phys. Chem. B* **2007**, *111*, 191−198.
(54) Dominguez, G.; Wilkins, G.; Thiemens, M. H. The Soret effect and isotropic fractionation in high-temperature silicate melts. *Nature* **2011**, *473*, 70−73.
(55) Huang, F.; Chakraborty, P.; Lundstrom, C. C.; Holmden, C.; Glessner, J. J. G.; Kieffer, S. W.; Lesher, C. E. Isotope fractionation in silicate melts by thermal diffusion. *Nature* **2010**, *464*, 396−400.
(56) Shimizu, M.; Matsuoka, J.; Kato, H.; Nishi, M.; Visbal, H.; Nagashima, K.; Sakakura, M.; Shimotsuma, Y.; Itasaka, H.; Hirao, K.; Miura, K. Role of partial molar enthalpy of oxides on Soret effect in high temperature CaO-SiO_2 melts. *Sci. Rep.* **2018**, *8*, 15489−15489.
(57) Lacks, D. J.; Goel, G.; Bopp, C. J.; van Orman, J. A.; Lesher, C. E.; Lundstrom, C. C. Lundstrom, Isotope Fractionation by Thermal Diffusion in Silicate Melts. *Phys. Rev. Lett.* **2012**, *108*, No. 065901.
(58) Alonso de Mezquia, D.; Mounir Bou-Ali, M.; Madariaga, J. A.; Santamaría, C. Mass effect on the Soret coefficient in n-alkane mixtures. *J. Chem. Phys.* **2014**, *140*, No. 084503.
(59) http://www.castep.org/
(60) https://www.gromacs.org/

https://doi.org/10.1021/acsomega.1c04926
ACS Omega 2022, 7, 518−527